A Full-Wave Analysis Model for Uniplanar Circuits with Lumped Elements

Chi-Hsueh Wang, Huei Wang, *Senior Member, IEEE*, and Chun Hsiung Chen, *Fellow, IEEE*

***Abstract*—A full-wave analysis model, which uses the current–source port concept for combined electromagnetic and circuit simulation of linear and nonlinear uniplanar circuits is proposed. The passive distributed parts of the circuit are analyzed by the mixed-potential integral-equation formulation, and the connections between distributed parts and lumped elements are treated by the current–source ports. Based on this model, all electromagnetic effects associated with the distributed circuit parts, as well as the interactions between lumped elements (active or passive) and distributed elements (passive) can easily be characterized. In this study, the proposed model is tested by applying it to the problems with a chip capacitor, spiral inductor, and active slot antenna. The model is then employed to design and analyze two novel uniplanar mixers. The simulation results are also validated by the measurements.**

***Index Terms*—Full-wave analysis, singly balanced mixer, uniplanar circuit.**

I. Introduction

SIMULATIONS of circuit components are essential in predicting the performance of a complex system and in providing an optimum circuit design. In a conventional design procedure, a complicated circuit is separated into several subcircuits, which are then recombined after each subcircuit is simulated individually. This technique may be adequate in providing useful results for a circuit design. However, as the circuit becomes more and more complex and the operating frequency is increased, it would be difficult to divide the circuit into several well-defined subcircuits due to the essential electromagnetic coupling between each subcircuit. Thus, a combined analysis of the whole circuit, which includes the distributed and lumped elements, is of necessity. Especially in the monolithic microwave integrated circuit (MMIC) process, the implementation of a highly integrated circuit needs more accurate simulation results at the initial design stage because further tuning after fabrication is not practical.

Microstrip lines are widely used in implementing the microwave circuits, for which several full-wave analysis algorithms have been developed. Some microstrip circuits with lumped elements have been analyzed, using the extended finite-difference time-domain (FDTD) approach [1]–[3]. Specifically, by using the equivalent sources, the device–wave interaction may be characterized and incorporated into the FDTD time-marching scheme. The linear and nonlinear phenomena may be examined by employing a large-signal device circuit model, and the analysis of electromagnetic compatibility (EMC) and electromagnetic interference (EMI) effects may also be included. By the same concept, an analysis model was also realized by using the global finite-element time-domain method [4], [5], which gave good accuracy when compared with the extended FDTD approach.

Microstrip circuits may also be analyzed globally using the frequency-domain methods. An algorithm to extend the capabilities of the finite-element method to treat lumped elements was reported in [6]. It made use of the port-based concept, by which the edge unknowns connected to the lumped elements are defined as the circuit ports so as to combine the distributed parts with the device parts. Recently, a space-domain technique [7] was proposed to provide an analysis tool for a nonlinear circuit. By this voltage–source port formulation, one can design and analyze each subcircuit of a complex circuit independently, and then combine them through the ports in the final simulation process. Although the formulation is simple, it exhibits some numerical difficulties when lumped elements are involved. Specifically, a numerical error may be generated when the voltage–source port is treated by a half basis, which introduces an undesired numerical discontinuity effect [8]. Another kind of error is induced by assuming that the lumped element is inserted into an infinitesimal gap, and using the full basis to handle the voltage–source port. This infinitesimal gap assumption would introduce another numerically induced capacitance effect that is strongly dependent on the mesh size [7] and can dramatically spoil the results. For this reason, a correction procedure to reduce such a numerically induced capacitance was developed [7].

Uniplanar circuits which make use of a coplanar waveguide (CPW) and slotline receive increased attention due to the merits such as elimination of the backside processes, simple realization of series and shunt circuit components, and easy integration with other lumped or active elements [9]. These uniplanar circuits can also be designed by dividing the whole circuit into several subcircuits, which are then treated separately. Sometimes the electromagnetic coupling and discontinuity effects associated with the circuit are not negligible, and then a global full-wave analysis model is urgently needed.

A more complete global analysis of a uniplanar circuit may be conducted by using a coupled system of Boltzmann's transport equations for carrier transport phenomena and Maxwell's equations for lumped devices and distributed parts of the circuit [10], [11]. This global analysis needs intensive computer-memory requirement and large simulation time, and these difficulties may partly be reduced by the hybridization approach [11].

Manuscript received November 5, 2001. This work was supported by the Ministry of Education and by the National Science Council of Taiwan, R.O.C., under Grant 89-E-FA06-2-4 and Grant NSC 90-2219-E-002-003.

The authors are with the Department of Electrical Engineering, Graduate Institute of Communication Engineering, National Taiwan University, Taipei 106, Taiwan, R.O.C. (e-mail: chchen@ew.ee.ntu.edu.tw).

Digital Object Identifier 10.1109/TMTT.2002.806903

The simplified analysis approaches for microstrip circuits may also be extended to the uniplanar circuits. By coupling the equivalent current sources with the extended FDTD approach, the packaging and crosstalk effects for a CPW linear amplifier were discussed by Ma *et al.* [3]. Vourch *et al.* [12] employed the space-domain technique to design a uniplanar active antenna. However, the research on uniplanar circuits with lumped elements is relatively limited.

In this paper, a space-domain full-wave analysis model that adopts the current–source port in the formulation is proposed instead of using the voltage–source port in which the voltage is regarded as a variable [7]. The proposed model is based on the mixed-potential integral-equation formulation, which uses the method of moment to solve the magnetic current distributions on the apertures and uses the overlapping rooftop basis functions to expand these unknown magnetic currents. Two advantages are associated with this full-wave analysis model. By dealing with the unknown magnetic currents, the developed algorithm is easy to handle the uniplanar circuits. Next, with the removal of the infinitesimal gap assumption, the current–source ports may be located at the positions where the lumped elements are inserted, thus, the proposed model can naturally take care of the lumped-element effect instead of regarding the lumped element as a numerical box [12]. Based on this current–source port concept, the model is tested by applying it to the problems with a chip capacitor, spiral inductor, and active slot antenna. The model is then employed to design and analyze two novel uniplanar mixers. The simulation results are also validated by the measurements.

II. Full-Wave Analysis Model

Analysis of uniplanar circuits such as the CPW discontinuity structures with linear or nonlinear lumped elements inserted over the CPW slots [see Fig. 1(a)] is the main concern of this study. The lumped elements under consideration include resistors, capacitors, inductors, diodes, and transistors.

Theoretically, the proposed full-wave analysis model is based on the mixed-potential integral equation [13]

$$\hat{z}\times\vec{H}^{\rm ex}(\vec{r}) = \hat{z}\times\left[\int\!\!\int_S j\omega\overline{\overline{G}}_F(\vec{r}|\vec{r}')\cdot\vec{M}_s(\vec{r}')ds' + \int_S\int\nabla G_\phi(\vec{r}|\vec{r}')q_{ms}(\vec{r}')ds'\right]. \quad (1)$$

Here, $\vec{H}^{\rm ex}$ is the known excitation magnetic field, $\overline{\overline{G}}_F$ and G_ϕ are the Green's functions for the CPW structure, and $\vec{M}_s$ and q_{ms} are the equivalent surface magnetic currents and surface magnetic charges over the CPW apertures, respectively. In the Galerkin's moment-method procedure, the overlapping rooftop basis functions are used to expand the unknown surface magnetic current

$$M_s(\vec{r}') = \sum_{m=1}^{N} e_m\Lambda_m(\vec{r}') \quad (2)$$

where e_m are the unknown coefficients and $\Lambda_m(\vec{r}')$ are the known rooftop basis functions.

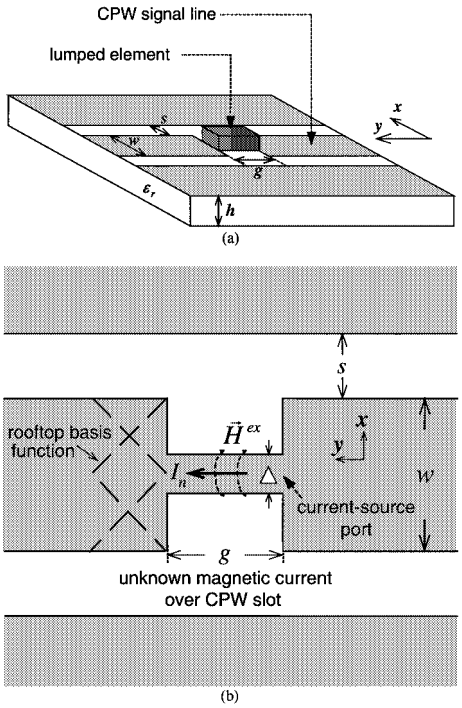

Fig. 1. (a) Geometry of lumped-element problem. (b) Configuration of current–source port in the formulation.

In this formulation, the excitation magnetic field is represented by a current–source port, which is imposed across a gap where the lumped element is located. The current–source port configuration is shown in Fig.1(b) in which the excitation magnetic field $\vec{H}^{\rm ex}$ is expressed in terms of the source current I_n as

$$H^{\rm ex}(\vec{r}) = \frac{I_n}{\Delta}. \quad (3)$$

Thus, the inner product of the excitation term can be written as

$$\int\!\!\int_{S_m}\Lambda_m(\vec{r})H^{\rm ex}(\vec{r})ds = \delta_{mn}I_n. \quad (4)$$

Note that the source currents associated with the excitation ports, where the lumped elements are located, are regarded as variables and all the other inner product terms are set to zero.

The concepts of the voltage–source and current–source ports should be clarified. In the voltage–source port formulation [7], the lumped element is connected to the left- and right-hand sides of rooftop basis functions so that a gap is introduced across the port, which would make the basis discontinuous and induce some numerical errors. In the current–source port formulation, the directions of electric source current and magnetic current are perpendicular to each other so that the introduction of a gap across the port still keeps the basis continuous.

Based on the current–source port formulation, the integral equation (1) may be converted into a matrix equation

$$\begin{bmatrix} Y^{pp} & Y^{pc} \\ Y^{cp} & Y^{cc}\end{bmatrix}\cdot\begin{bmatrix} V^p \\ V^c\end{bmatrix} = \begin{bmatrix} I^p \\ 0\end{bmatrix} \quad (5)$$

where V and I are the column vectors associated with the coefficients of basis functions and excitation currents. The superscripts p and c refer to the current–source ports and the other

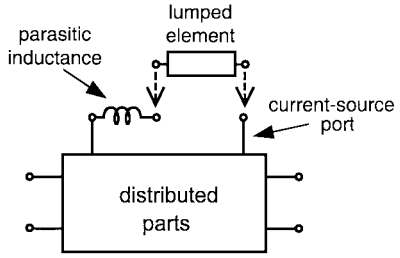

Fig. 2. Current–source port for connecting distributed parts and lumped element.

parts of the circuit, respectively. The admittance matrix equation in (5) can further be simplified to

$$\left[Y^{\text{total}}\right] \cdot [V^p] = [I^p] \tag{6}$$

where

$$\left[Y^{\text{total}}\right] = [Y^{pp}] - [Y^{pc}] \cdot [Y^{pc}]^{-1} \cdot [Y^{cp}]. \tag{7}$$

Physically, the admittance matrix $\left[Y^{\text{total}}\right]$ may characterize the complicated phenomena associated with the distributed parts of the circuit. Specifically, each excitation is represented by a current–source port, and the excitation port current I_n is regarded as an unknown without additional numerical computation [7]. After the admittance matrix $\left[Y^{\text{total}}\right]$ is established and connected to the lumped elements associated with the current–source ports, the whole circuit is then simulated by the circuit-simulation software, which supplies the required tool for simulating the complex circuits.

Although the proposed full-wave analysis model can handle the uniplanar circuit structure by removing the infinitesimal gap assumption $(\text{g} \to 0)$, it may suffer from some numerical difficulties when the current–source port concept is employed. The current–source port to connect the distributed parts of a circuit to the lumped element is represented by Fig. 2. Here, a series inductance is numerically induced by the thin current–source assumption $(\Delta \to 0)$ and the value of this inductance depends on the mesh size. Thus, a correction procedure to reduce the error due to this numerically induced inductance would be essential in the subsequent numerical simulation.

III. Model Validation

As a test of the full-wave analysis model, it is first applied to the analysis of the passive-element problem associated with a chip capacitor $(C = 1\,\text{pF})$, which contains a parasitic series inductance $L \fallingdotseq 0.83\,\text{nH}$. Fig. 1(a) shows the simulated structure in which the lumped element is replaced by the chip capacitor. The simulation is conducted, using the current–source port to connect the lumped element and the distributed parts, and then analyzing the whole circuit by the circuit simulation tool Libra. Fig. 3(a) shows the simulated results (without correction) for this problem and, for comparison, the measured results are also included. Due to the presence of parasitic series inductance, the measured results exhibit a resonance around 7.2 GHz. Without correction, the simulated results show some numerical errors and predict a resonance around 3.5 GHz because additional numerically induced inductance is generated. Fig. 3(b) shows the

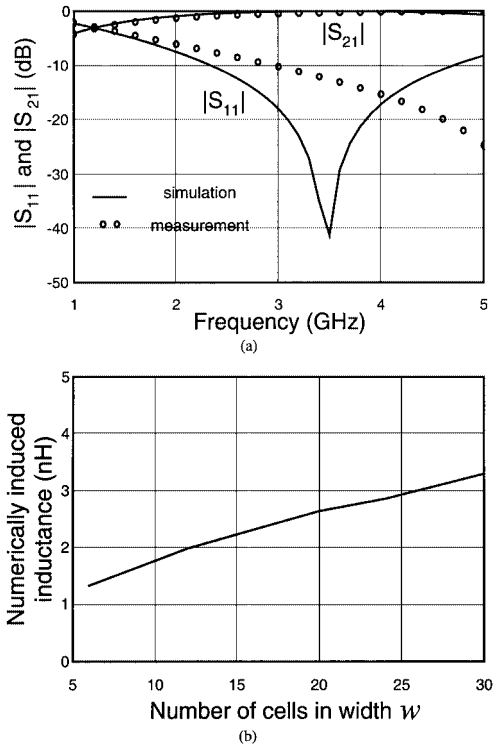

Fig. 3. (a) Simulated results (without correction) for chip capacitor problem (capacitance = 1 pF). (b) Numerically induced inductance for different number of cells in width w.

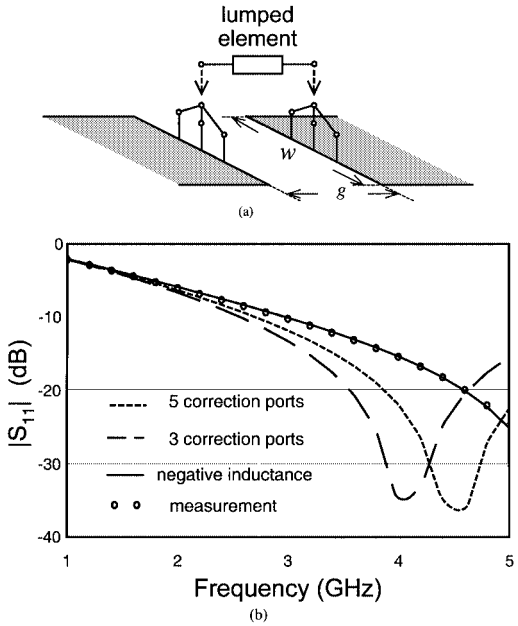

Fig. 4. (a) Multiport correction procedure in current–source port formulation. (b) Simulated results (with correction) for chip-capacitor problem.

value of numerically induced inductance for different number of cells in width used in the current–source port simulation.

The error due to numerically induced inductance might be reduced by connecting a negative series inductance to the current–source port, with the magnitude of the negative inductance equal to the numerically induced inductance. This method is not practical in circuit design because an additional simulation is needed to get the value of the numerically induced inductance.

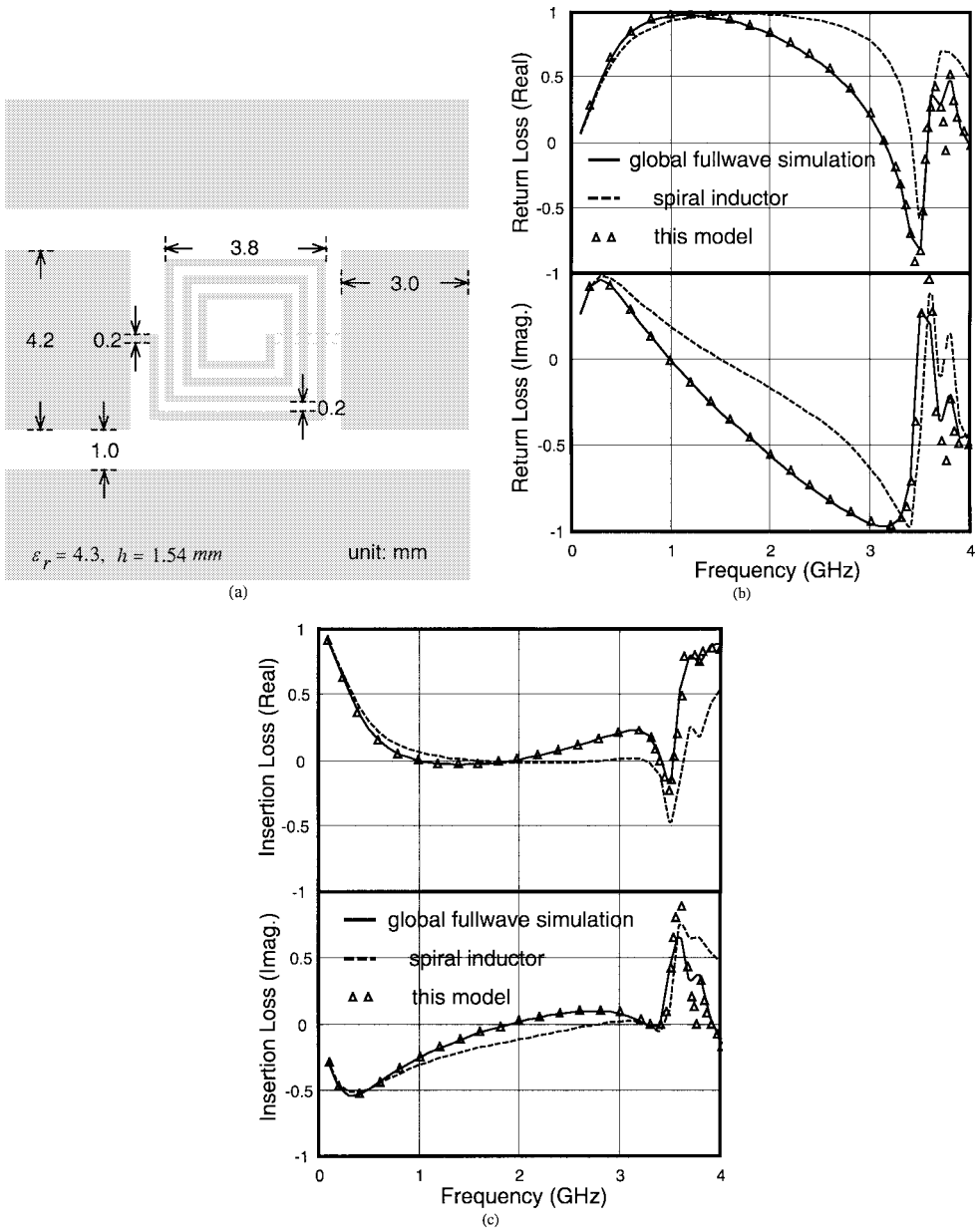

Fig. 5. (a) Geometry of spiral-inductor problem and simulated results for spiral-inductor problem. (b) Return loss. (c) Insertion loss.

In this study, a correction procedure for reducing this numerically induced inductance effect is proposed using the multiport concept, as shown in Fig. 4(a), in which all current–source ports are parallelly connected to the lumped element (capacitor). The numerically induced inductance effect would be reduced by shunting the ports to each other. The solid line in Fig. 4(b) shows the simulated results of including the negative inductance, which agree well with the measured ones. The broken line in Fig. 4(b) depicts the simulated results by connecting three correction ports to the capacitor, and the dashed line shows the results simulated by five correction ports. Note that the error due to numerically induced inductance is reduced when the number of correction ports is increased. In addition to the reduction in the numerically induced inductance effect, this multiport correction procedure can also be used to discuss the influence of the lumped-element size, and its effect is important especially in high frequency.

By the proposed full-wave analysis model, together with the multiport correction procedure, another passive-element problem with a spiral inductor inserted in the CPW signal line gap [see Fig. 5(a)] is tested. To confirm the accuracy of the proposed model, the following simulations are conducted. First, the whole structure shown in Fig. 5(a) is simulated by the global full-wave analysis technique [13]. Next, the spiral inductor along is simulated by the same full-wave algorithm from which one obtains the values of inductance and parasitic capacitance as 43.84 nH and 0.044 pF, respectively. Finally, the spiral inductor is connected to the CPW line, and the combined (or whole) structure in Fig. 5(a) is simulated by the proposed full-wave analysis model with multiport correction procedure. Here, five ports are used in the correction procedure. In Fig. 5(b) and (c), the simulated results for the whole structure by the global full-wave analysis technique are represented by the solid lines and those by the proposed model are denoted by

the symbol Δ. The full-wave simulated results for the spiral inductor along are also included in Fig. 5(b) and Fig. 5(c) for comparison. The results of the proposed model agree very well with those of the global full-wave simulation. By comparing with the results for the single spiral inductor, the influence of actual physical gap and discontinuity effects cannot be neglected. The agreement in the results for the whole structure by two different methods implies that the gap and discontinuity effects can be well treated by the proposed model. Here, the capacitance of the actual physical gap between CPW signal lines is approximately 0.15 pF. Note that it needs 409 unknowns to describe the whole structure [see Fig. 5(a)] by the global full-wave analysis technique, and it only needs 375 unknowns (248 unknowns in the CPW line structure and 127 unknowns in the spiral inductor) by the proposed model. In most cases, the inserted element, e.g., a transistor or a diode, is always simulated by its equivalent-circuit model, which consumes less memory and CPW time.

For further verification, the active antenna problem discussed in [12] is also simulated by the proposed full-wave analysis model with a multiport correction procedure. Fig. 6(a) shows the layout of the CPW-fed active slot antenna. The matching sections in the active antenna circuit are designed so as to get a maximum gain at the operating frequency. In our simulation, four current–source ports are used to model the bipolar amplifier, which is represented by its manufacturer's equivalent-circuit model. The last step in simulation is to connect the distributed parts with the current–source ports for the bipolar amplifier, and then to analyze the active antenna circuit by the circuit simulation tool Libra. Fig. 6(b) shows the simulated results, by the proposed model, which are also compared with the measured and calculated ones of [12]. It turns out that our simulated results agree well with the measured ones and even better than the calculated ones of [12].

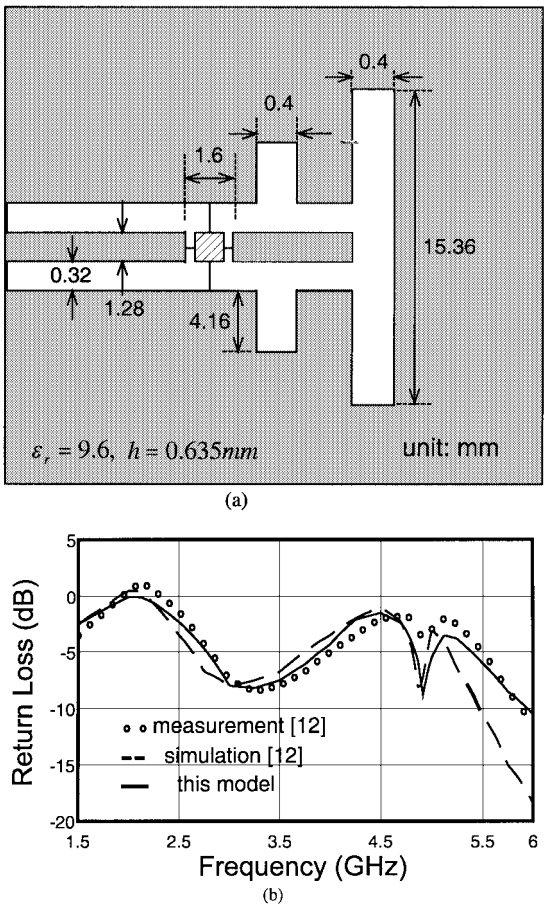

Fig. 6. (a) Layout of active slot antenna. (b) Corresponding simulated and measured results.

IV. UNIPLANARBALANCED MIXERS

The proposed full-wave analysis model together with the multiport correction procedure is employed to design and analyze two novel uniplanar balanced mixers. In these designs, the 180° hybrids are realized by the slotline-to-CPW junctions, which are useful components due to their simple architecture and attractive small circuit size. Sections IV-A and B show two types of slotline-to-CPW junctions in developing the uniplanar mixers discussed below.

A. Singly Balanced Fundamental Diode Mixer

The slotline-to-CPW junction [see Fig. 7(a)] directly connects the slotline to the CPW line. Here, an air bridge is introduced at a distance d_2 from the junction. To give an optimum design of the singly balanced fundamental diode mixer (Fig. 8), the influence of the air-bridge location on the characteristics of the S-parameters $|S_{31}|$ and $|S_{32}|$ must be examined. Through the junction, the signal from the slotline is converted into the coupled-slot mode along the CPW line, which would be shorted when it is propagated through the junction and meets the air bridge. The power transfer from port 1 to ports 3 and 4 would be a maximum around the frequency at which the length d_2 is equal to a quarter-wavelength $(\lambda/4)$. In the simulation of the junction in Fig. 7(a), the discontinuity effect of the air bridge has been taken into account. Fig. 7(b) shows the effect of the length d_2 on the S-parameters $|S_{31}|$ and $|S_{32}|$. It is clear that the passband of $|S_{31}|$ shifts as the length d_2 is varied. The signal from port 2, which is carried by the CPW mode, would transfer an equal amount of powers into ports 3 and 4 in a broad frequency range due to the little influence of the air bridge on the CPW mode. The simulated $|S_{32}|$ in Fig. 7(b) does reveal that the variation in d_2 has a negligible effect on the CPW mode signal from port 2. The coupled-slotline mode and CPW mode propagated along the CPW are uncoupled, leading to a very good isolation between ports 1 and 2. By using the slotline-to-CPW junction, shown in Fig. 7(a), a singly balanced fundamental diode mixer (Fig. 8) was developed in [14].

Fig. 8 shows the layout of a 180° singly balanced diode mixer. This uniplanar structure allows for simple grounding without via-holes and all the components are located on the same substrate side. In this design, the twin-spiral CPW-to-slotline transition [15] and the slotline-to-CPW junction in Fig. 7(a) are used to replace the traditional 180° hybrid. A series diode pair is mounted across the junction of the slotline. In the local oscillator (LO) port, matched sections of lengths d_3 and d_4 are used to ensure the satisfactory power transfer from LO port to the diode pair. The LO high-pass filter is realized by a chip-capacitor C and the IF low-pass filter by a solenoid-inductor L.

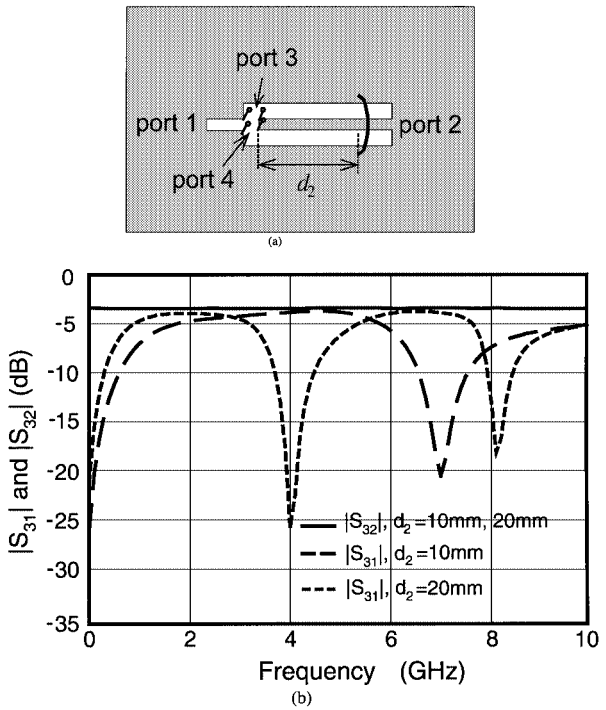

Fig. 7. (a) Configuration of slotline-to-CPW junction. (b) Effect of the length d_2 on $|S_{31}|$ and $|S_{32}|$.

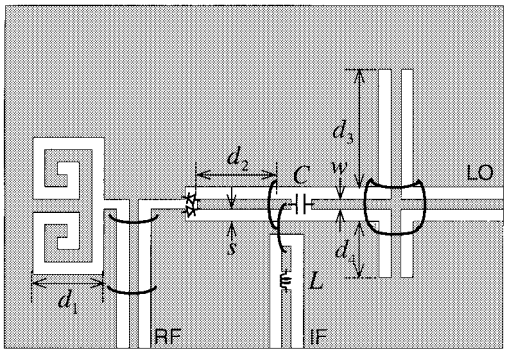

Fig. 8. Geometry of a 180° singly balanced fundamental diode mixer ($s = 1.0$ mm, $w = 0.75$ mm, $d_1 = 7$ mm, $d_2 = 12$ mm, $d_3 = 25$ mm, $d_4 = 9.5$ mm, $C = 9$ pF, $L = 25$ nH, $\varepsilon_r = 4.3$, $h = 1.54$ mm).

The twin-spiral transition [15] is adopted due to its wide bandwidth and small size requirement. This transition can achieve a size that is 1/3 of the conventional CPW-to-slotline transition and has a 2.55 : 1 bandwidth.

Functionally similar to the 180° hybrid, the slotline-to-CPW junction converts an RF signal along the slotline into two signals (equal amplitudes, but 180° out of phases) associated with the coupled slotline mode of the CPW line. In addition to creating 180° out-of-phase RF signals on the series diode pair, the slotline-to-CPW junction in Fig. 7(a) also guarantees excellent isolations between the RF/LO and RF/IF ports. This is due to the uncoupling feature of the RF signal (slotline mode) and LO signal (CPW mode).

Conventionally, the slotline-to-CPW junction and diode pair in the mixer may be analyzed simply by incorporating the circuit model for diode pair into the transmission-line models for the slot line and CPW line [16]. This equivalent transmission-line circuit model is too simple to take care of the parasitic effect and mode-coupling effect. Especially when the slotline-to-CPW junction is more complicated and the diode pair is so close to the junction, the influence of the parasitic effects, such as the discontinuity effect of the junction, as well as the interaction between the junction and diode pair, would become significant. A method to avoid such an interaction effect might be achieved by leaving the diode pair far from the junction [17], and this would make the circuit size become bigger.

In order to optimize the mixer performance and to minimize the circuit size, the series diode pair in Fig. 8 should be located as close to the slotline-to-CPW junction as possible. For this circuit, it is not enough to simulate the slotline-to-CPW junction and diode pair merely by the conventional equivalent transmission-line circuit model [16], which does not include the discontinuity effect across the junction. In this study, the slotline-to-CPW junction and diode pair combined together are analyzed by the proposed full-wave analysis model, which combines the current–source port concept and the harmonic-balance method in the final simulation. The slotline-to-CPW junction can then be regarded as a five-port subnetwork, which is then connected to the current–source ports associated with the diode pair. The first port is the slotline connected to the twin-spiral transition. The other two ports are the CPW line to support the CPW mode and coupled slotline mode, respectively. The diode pair, which is connected to the remaining two ports, is discussed by the manufacturer's equivalent-circuit model. By this combined model, all the parasitic effects can naturally be handled.

The length d_2 and the bandwidth of twin-spiral transition are essential in determining the bandwidth of the mixer. Better transfer of RF power into two diodes may be achieved by taking the length d_2 around $\lambda/4$ of the RF signal.

The proposed full-wave analysis model may also be used in the simulation of the LO and IF filters, which are realized by the capacitor C and inductor L. Their parasitic discontinuity effects are very small, thus, the equivalent transmission-line circuit model [16] is also adequate in dealing with the filter circuits.

Shown in Fig. 9(a)–(d) are the simulated and measured results for the diode mixer shown in Fig. 8. The mixer is fabricated on the FR4 substrate whose dielectric constant $\varepsilon_r = 4.3$ and thickness $h = 1.54$ mm. Here, the length d_2 is not exactly $\lambda/4$ at the center frequency of 2.5 GHz due to the discontinuity effect. For the measurement setup, the RF and LO sources are given by the network analyzer HP8722C and signal generator 83620A, respectively. The IF signal power is measured by the GiGa power meter 8542B and power sensor. This mixer exhibits a conversion loss of 5∼7 dB for an LO signal of 2.7 dBm when the RF signal is swept from 2 to 3 GHz, and the best is at 2.4 GHz. The conversion loss begins to saturate around 1 dBm of LO input power and changes very little above 3 dBm. Fig. 9(d) shows the corresponding LO-to-IF isolation versus LO frequency, which is better than 19 dB.

B. Singly Balanced Subharmonic Diode Mixer

Fig. 10(a) shows a modified version of the slotline-to-CPW junction. Comparing with the one in Fig. 7(a), the modified structure has a similar behavior in $|S_{31}|$, but it has a different response in $|S_{32}|$. To the coupled-slotline mode, the shorted stub

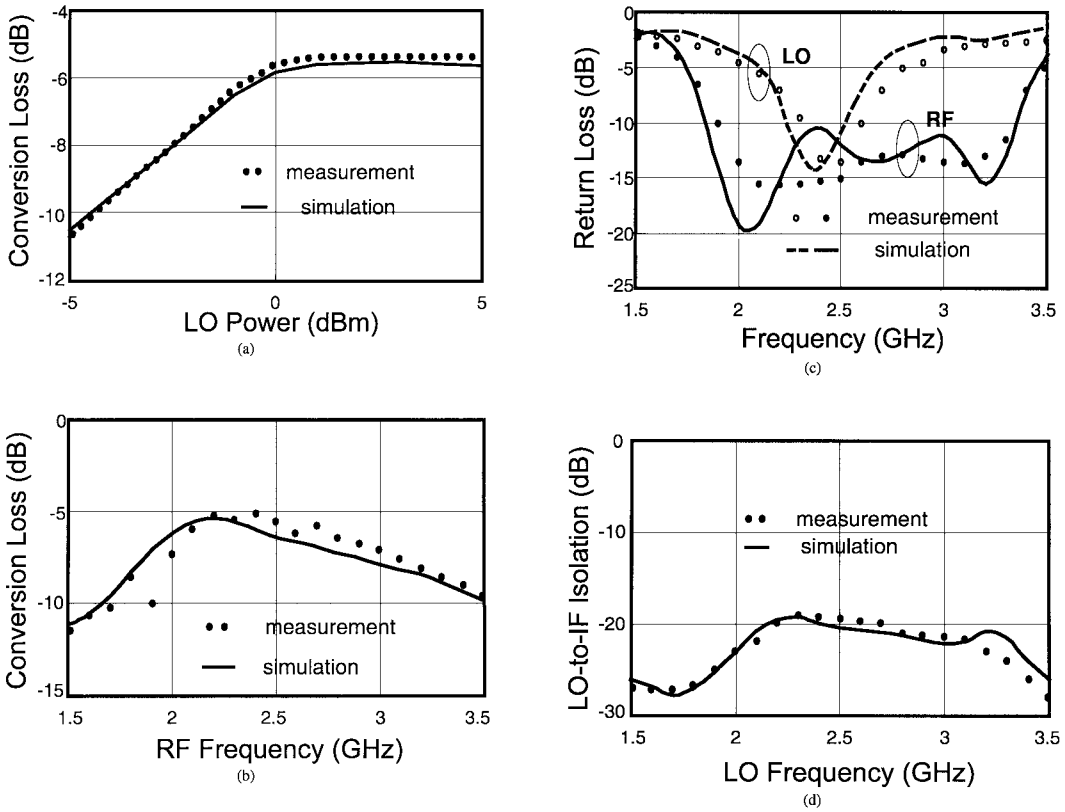

Fig. 9. Simulated and measured results for the fundamental diode mixer (Fig. 8). (a) and (b) Conversion loss. (c) Return loss. (d) LO-to-IF isolation. ($P_{LO} = 2.7$ dBm, $PRF = -10$ dBm).

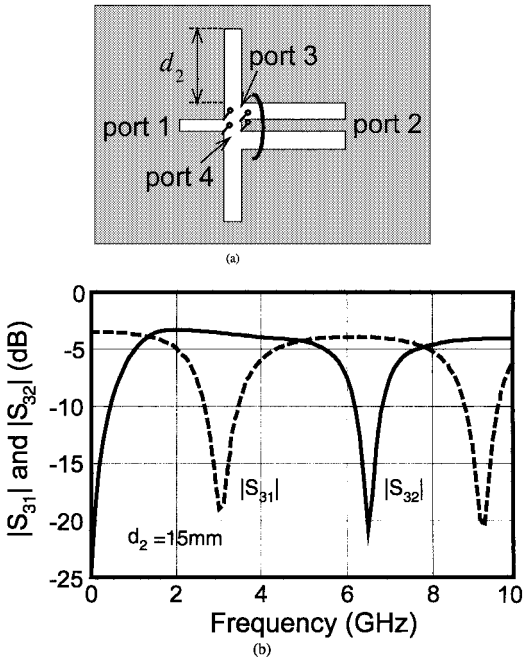

Fig. 10. (a) Configuration of modified slotline-to-CPW junction. (b) Simulated results for $|S_{31}|$ and $|S_{32}|$.

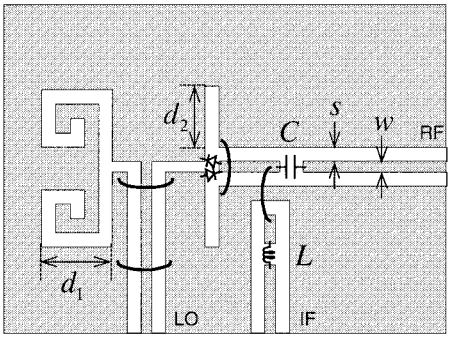

Fig. 11. Geometry of singly balanced subharmonic diode mixer. ($s = 1.0$ mm, $w = 0.7$ mm, $d_1 = 10$ mm, $d_2 = 12$ mm, $C = 5$ pF, $L = 67$ nH, $\varepsilon_r = 4.3$, $h = 1.54$ mm).

pair together with the air-bridge present similar functions, such as the one in Fig. 7(a) did. The slotline-mode signal from port 1 could propagate to ports 3 and 4 smoothly when the stub length d_2 is approximately $\lambda/4$ of the signal frequency from port 1. In this case, the stub pair may be treated as a shunt to the junction. On the contrary, for the CPW mode signal from port 2, the stub pair should be treated as the series ones to ports 3 and 4. Thus, the CPW-mode signal from port 2 would smoothly propagate to ports 3 and 4 as the stub length d_2 is approximately a half-wavelength $(\lambda/2)$ of the signal frequency from port 2. The simulated results of the junction in Fig. 10(a) are shown in Fig. 10(b). The effects of the stub pair on the coupled-slotline mode and CPW mode are completely different, thus, the passbands of $|S_{31}|$ and $|S_{32}|$ are different. Specifically, the passband of $|S_{32}|$ would be in the frequency range for which d_2 is around $\lambda/2$, and that of $|S_{31}|$ would be in the range for which d_2 is around $\lambda/4$. By this feature, a new strategy of suppressing the fundamental spurious response is accomplished by adopting the modified slotline-to-CPW junction in the design of a subharmonically pumped mixer.

Fig. 11 shows the topology of the singly balanced subharmonically pumped diode mixer based on the modified

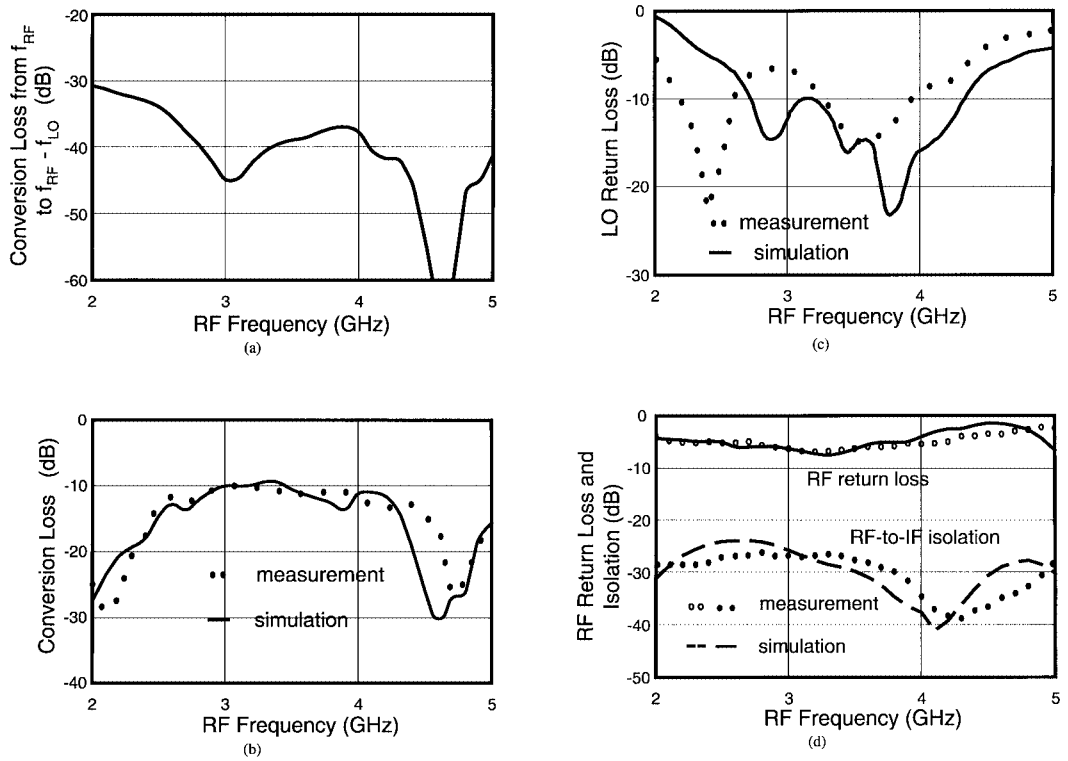

Fig. 12. Simulated and measured results for the subharmonic diode mixer (Fig. (11). (a) Simulated conversion loss of the signal from f_{RF} to $f_{RF} - f_{LO}$. (b) Conversion loss. (c) LO return loss. (d) RF return loss and RF-to-IF isolation ($P_{LO} = 5$ dBm, $P_{RF} = -10$ dBm).

slotline-to-CPW junction [see Fig. 10(a)]. The major components of this uniplanar mixer are the series diode pair, twin-spiral CPW-to-slotline transition [15], modified slotline-to-CPW junction of Fig. 10(a), and diplexer, which is realized by the capacitor C and inductor L.

In this design, the 180° hybrid is realized by the combination of twin-spiral CPW-to-slotline transition [15] and modified slotline-to-CPW junction. The stub length d_2 (in Fig. 11) is designed to be around $\lambda/4$ of the LO signal so that the LO signal, carried by the slotline mode, would transfer almost an equal amount of power into the diode pair. By the short-circuit action of the stub pair, the RF signal (carried by the CPW mode) will mainly couple to the diode pair when its frequency is two times the frequency of the LO signal. For the spurious signal with frequency $f_{RF} - f_{LO}$, which is close to the LO frequency, it would not reach the RF port and would be reflected by the open-circuit action of the stub pair when the length d_2 is around $\lambda/4$ of the spurious signal frequency. Fig. 12(a) shows the simulated conversion loss from the RF signal to the spurious signal of frequency $f_{RF} - f_{LO}$. It illustrates that the fundamental spurious response for $f_{RF} - f_{LO}$ is effectively suppressed by the use of the new structure in Fig. 10(a).

Fig. 12(b)–(d)shows the simulated and measured results of the subharmonic diode mixer shown in Fig. 11. The conversion loss smoothly varies from 10 to 12 dB when the RF signal is swept from 3 to 4 GHz and the IF frequency is 0.1 GHz. All the isolations are better than 25 dB.

V. Conclusion

A full-wave analysis model that uses the current–source port concept to deal with the linear and nonlinear uniplanar circuits has been established. By incorporating the multiport correction procedure into this model, the numerically induced inductance effect may be reduced in the simulation. This model can handle all the electromagnetic effects associated with the circuit structure, and can treat any linear or nonlinear and passive or active lumped element, especially when the element is close to the circuit discontinuity parts. Specifically, the proposed model can be applied to a complex circuit configuration with different kinds of lumped elements once the electromagnetic simulation for the distributed parts is conducted.

By adopting the modified slotline-to-CPW junction [see Fig. 10(a)] to the subharmonic diode mixer (Fig. 11), it has been shown that the fundamental spurious response of the signal with frequency $f_{RF} - f_{LO}$ is successfully suppressed. The design and analysis of the uniplanar singly balanced diode mixers reveal that the proposed model may give results in good agreement with the measurement. The model is easier in handling microwave circuits, especially with uniplanar structures.

References

[1] V. A. Thomas, M. E. Jones, M. Piket-May, A. Taflove, and E. Harrigan, "The use of SPICE lumped circuits as sub-grid models for FDTD analysis," *IEEE Microwave Guided Wave Lett.*, vol. 6, pp. 199–201, May 1996.

[2] C.-N. Kuo, B. Houshmand, and T. Itoh, "Full-wave analysis of packaged microwave circuits with active and nonlinear devices: an FDTD approach," *IEEE Trans. Microwave Theory Tech.*, vol. 45, pp. 819–826, May 1997.

[3] K.-P. Ma, M. Chen, B. Houshmand, Y. Qian, and T. Itoh, "Global time-domain full-wave analysis of microwave circuits involving highly nonlinear phenomena and EMC effects," *IEEE Trans. Microwave Theory Tech.*, vol. 47, pp. 859–866, June 1999.

[4] K. Guillouard, M. F. Wong, V. F. Hanna, and J. Citerne, "A new global time-domain electromagnetic simulator of microwave circuits including lumped elements based on finite-element method," *IEEE Trans. Microwave Theory Tech.*, vol. 47, pp. 2045–2049, Oct. 1999.
[5] S.-H. Chang, R. Coccioli, Y. Qian, and T. Itoh, "A global finite-element time-domain analysis of active nonlinear microwave circuits," *IEEE Trans. Microwave Theory Tech.*, vol. 47, pp. 2410–2416, Dec. 1999.
[6] K. Guillouard, M. F. Wong, V. F. Hanna, and J. Citerne, "A new global finite element analysis of microwave circuits including lumped elements," *IEEE Trans. Microwave Theory Tech.*, vol. 44, pp. 2587–2594, Dec. 1996.
[7] R. Gillard, S. Dauguet, and J. Citerne, "Correction procedures for the numerical parasitic elements associated with lumped elements in global electromagnetic simulators," *IEEE Trans. Microwave Theory Tech.*, vol. 46, pp. 1298–1306, Sept. 1998.
[8] M. I. Aksun and R. Mittra, "Estimation of spurious radiation from microstrip etches using closed-form Green's functions," *IEEE Trans. Microwave Theory Tech.*, vol. 40, pp. 2063–2069, Nov. 1992.
[9] K. C. Gupta, R. Garg, and I. J. Bahl, *Microstrip Lines and Slotlines*, 2nd ed. Norwood, MA: Artech House, 1996.
[10] M. A. Alsunaidi, S. M. S. Imtiaz, and S. M. El-Ghazaly, "Electromagnetic wave effects on microwave transistors using a full-wave time-domain model," *IEEE Trans. Microwave Theory Tech.*, vol. 44, pp. 799–808, June 1996.
[11] S. M. S. Imtiaz and S. M.Samir M. El-Ghazaly, "Global modeling of millimeter-wave circuits: Electromagnetic simulation of amplifiers," *IEEE Trans. Microwave Theory Tech.*, vol. 45, pp. 2208–2216, Dec. 1997.
[12] E. Vourch, M. Drissi, and J. Citerne, "A full-wave analysis of active uniplanar structures," in *IEEE AP-S Int. Symp. Dig.*, June 1995, pp. 1062–1065.
[13] J. Sercu, N. Fache, F. Libbrecht, and P. Lagasse, "Mixed potential integral equation technique for hybrid microstrip-slotline multilayered circuits using a mixed rectangular-triangular mesh," *IEEE Trans. Microwave Theory Tech.*, vol. 43, pp. 1162–1172, May 1995.
[14] C.-H. Wang, H. Wang, and C. H. Chen, "A new global-analysis model for microwave circuits with lumped elements," in *IEEE MTT-S Int. Microwave Symp. Dig.*, May 2001, pp. 1937–1940.
[15] Y. S. Lin and C. H. Chen, "Design and modeling of twin-spiral coplanar-waveguide-to-slotline transitions," *IEEE Trans. Microwave Theory Tech.*, vol. 48, pp. 463–466, Mar. 2000.
[16] P. C. Hsu, C. Nguyen, and M. Kintis, "Design and performance of a new uniplanar diode mixer," *IEEE Microwave Guided Wave Lett.*, vol. 10, pp. 192–194, May 2000.
[17] H. Gu and K. Wu, "A novel uniplanar balanced subharmonically pumped mixer for low-cost broadband millimeter-wave transceiver design," in *IEEE MTT-S Int. Microwave Symp. Dig.*, June 2000, pp. 635–638.

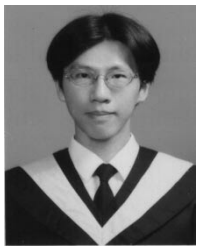

Chi-Hsueh Wang was born in Kaohsiung, Taiwan, R.O.C., in 1976. He received the B.S. degree in electrical engineering from the National Cheng Kung University, Tainan, Taiwan, R.O.C., in 1997, and is currently working toward the Ph.D. degree in communication engineering at the National Taiwan University, Taipei, Taiwan, R.O.C.

His research interests include the design and analysis of microwave and millimeter-wave circuits and computational electromagnetics.

Huei Wang (S'83–M'83–SM'95) was born in Tainan, Taiwan, R.O.C., on March 9, 1958. He received the B.S. degree in electrical engineering from the National Taiwan University, Taipei, Taiwan, R.O.C., in 1980, and the M.S. and Ph.D. degrees in electrical engineering from Michigan State University, East Lansing, in 1984 and 1987, respectively.

During his graduate study, he was engaged in research on theoretical and numerical analysis of electromagnetic radiation and scattering problems. He was also involved in the development of microwave remote detecting/sensing systems. In 1987, he joined the Electronic Systems and Technology Division, TRW Inc. He was a Member of the Technical Staff and Staff Engineer responsible for MMIC modeling of computer-aided design (CAD) tools, MMIC testing evaluation, and design. He then became the Senior Section Manager of the Millimeter Wave Sensor Product Section, RF Product Center, TRW Inc. In 1993, he visited the Institute of Electronics, National Chiao-Tung University, Hsin-Chu, Taiwan, R.O.C., and taught MMIC-related topics. In 1994, he returned to TRW Inc. In February 1998, he joined the faculty of the Department of Electrical Engineering, National Taiwan University, where he is currently a Professor.

Dr. Wang is a member of Phi Kappa Phi and Tau Beta Pi.

Chun Hsiung Chen (SM'88–F'96) was born in Taipei, Taiwan, R.O.C., on March 7, 1937. He received the B.S.E.E. and Ph.D. degrees in electrical engineering from the National Taiwan University, Taipei, Taiwan, R.O.C., in 1960 and 1972, respectively, and the M.S.E.E. degree from the National Chiao Tung University, Hsinchu, Taiwan, R.O.C., in 1962.

In 1963, he joined the Faculty of the Department of Electrical Engineering, National Taiwan University, where he is currently a Professor. From August 1982 to July 1985, he was Chairman of the Department of Electrical Engineering at the same university. From August 1992 to July 1996, he was the Director of the University Computer Center. In 1974, he was a Visiting Scholar with the Department of Electrical Engineering and Computer Sciences, University of California at Berkeley. From August 1986 to July 1987, he was a Visiting Professor with the Department of Electrical Engineering, University of Houston, Texas. In 1989, 1990, and 1994, he visited the Microwave Department, Technical University of Munich, Munich, Germany, the Laboratoire d'Optique Electromagnetique, Faculte des Sciences et Techniques de Saint-Jerome, Universite d'Aix-Marseille III, Marseille, France, and the Department of Electrical Engineering, Michigan State University, East Lansing, respectively. His areas of interest include microwave circuit analysis and computational electromagnetics.